Ceramics International 49 (2023) 5872–5883

Contents lists available at ScienceDirect

Ceramics International

journal homepage: www.elsevier.com/locate/ceramint

Study of Eu^{3+}–Gd^{3+} co-doped Ba–Bi–B glasses for red-laser applications: Physical, structural, photoluminescence and time-resolved spectral characteristics

Devarajulu Gelija [a], B. Kiran Kumar [b,c], P. Reddi Babu [b], Yuwaraj K. Kshetri [d], Tae-Ho Kim [d], B. Deva Prasad Raju [b,**], Moon-Deock Kim [a,e,*]

[a] Institute of Quantum Systems (IQS), Chungnam National University, 99Daehak-ro, Yuseong-gu, Daejeon, 34134, Republic of Korea
[b] Department of Physics, Sri Venkateswara University, Tirupati, 517 502, India
[c] Department of Physics, Government Degree College, Rayachoty, 516 269, India
[d] Research Center for Green Advance Materials, Sun Moon University, Chungnam, 31460, Republic of Korea
[e] Department of Physics, Chungnam National University, 99Daehak-ro, Yuseong-gu, Daejeon, 34134, Republic of Korea

ARTICLE INFO

Keywords:
Eu^{3+}/Gd^{3+} ions
Barium–bismuth-borate glasses
Photoluminescence
Energy transfer
Time-resolved spectroscopy
Display devices

ABSTRACT

A series of Eu^{3+} and Eu^{3+}/Gd^{3+} co-doped barium-bismuth-borate (Ba–Bi–B) glasses were prepared by melt-quench technique. And deliberated the physical, structural, and spectroscopic properties of all glasses and explored the energy transfer process from Gd^{3+} to Eu^{3+} ions. The density of glasses increased with increasing of Gd^{3+} concentration in co-doped glasses. Characteristics of steady-state and time-resolved photoluminescence (PL) of Eu-doped and Eu^{3+}-Gd^{3+} co-doped glasses under different excitation wavelengths suggested the prospects of the investigated glass system for display device applications. PL spectrum displays a strong red emission peak centered at 612 nm due to the Eu^{3+}: $^5D_0 \rightarrow {}^7F_2$ transition. Less intense emissions centered at 577 nm ($^7F_0$), 590 nm ($^7F_1$), 651 nm ($^7F_3$) and 700 nm ($^7F_4$) are also observed from the radiative transitions of the excited state $^5D_0$ of Eu^{3+}ions. The values of radiative parameters such as transition probability, branching ratios, and stimulated emission cross-sections were obtained from Judd–Ofelt theory analysis and indicated the aptness of the Ba–Bi–B glasses for optical devices. A 5-fold enhancement in the PL intensity was observed in 1.0 mol% Eu^{3+} and 3.0 mol % Gd^{3+} co-doped glass under $\lambda_{Exci.} = 394$ nm excitation. The calculated commission Internationale de l'eclairage color coordinates and correlated color temperature values show that the Ba–Bi–B glasses are useful for red-laser and display device applications.

1. Introduction

Trivalent rare-earth (RE^{3+})-doped optical materials, glasses, crystals, phosphors, etc., play a significant role in photonic applications such as display devices, fiber lasers, up-conversion lasers, optical amplifiers, laser gain media and scintillators [1–6]. In the last few decades, glass materials have attracted researchers due to the ease of fabrication on large scale with required shape and sizes, optical homogeneity, high thermal stability, chemical stability, and also the large coefficient with the combination of RE^{3+} ions in the glass matrix.

The spectral behavior of RE (4f-4f) transitions and their performance for various applications depends on the composition of the glass host. Among the RE ions, the Eu^{3+} ion is special and has unique properties to examine the local ion symmetry of RE^{3+} ions in different glass systems. Eu^{3+} ions as optically active dopants predominantly produce the intense reddish-orange emission at 612 nm ($^5D_0 \rightarrow {}^7F_2$). This intense emission is a hypersensitive electronic transition ($^5D_0 \rightarrow {}^7F_2$) whose spectral characteristics have been investigated in different host matrices to obtain laser emission in the red spectral region and display devices [7–10].

In the recent past, different types of Eu^{3+}-doped glass materials were developed for optical displays, plasma display panels, visible lasers, and scintillation applications. For example, Nakamori et al. [11] prepared the Eu^{3+}-activated TeO_2–Al_2O_3–SrO glasses and studied scintillation properties. Yang et al. [12] investigated Eu^{3+} doped silicate glasses to

* Corresponding author. Institute of Quantum Systems (IQS), Chungnam National University, 99Daehak-ro, Yuseong-gu, Daejeon, 34134, Republic of Korea.
** Corresponding author.
E-mail addresses: drdevaprasadraju@gmail.com (B.D. Prasad Raju), mdkim@cnu.ac.kr (M.-D. Kim).

https://doi.org/10.1016/j.ceramint.2022.10.208
Received 4 August 2022; Received in revised form 19 September 2022; Accepted 15 October 2022
Available online 20 October 2022

Table 1
Nominal compositions of synthesized glasses (mol%).

Glass code	B_2O_3	Bi_2O_3	BaF_2	TiO_2	Eu_2O_3	Gd_2O_3
E0	45.0	15	30	10	0	0
E1	44.0	15	30	10	1.0	0
E1G0.5	43.5	15	30	10	1.0	0.5
E1G1.0	43.0	15	30	10	1.0	1.0
E1G2.0	42.0	15	30	10	1.0	2.0
E1G3.0	41.0	15	30	10	1.0	3.0

improve the efficiency of silicon solar cells. Venkatramu et al. [13] detailed optical and fluorescence properties of borate and fluoro borate doped zinc and lead glasses, Marimuthu et al. deliberated alkali borate glasses [14]. Similarly, several other glass systems as zinc-aluminum-bismuth borate glasses [15], 20PbO − 5CaO – 5ZnO – 10AF – 59B_2O_3 − 1Eu_2O_3 alkali borate glasses [16], alkali fluoroborate glasses [17], SiO2–B2O3–CaF2–NaF–Na2O glasses [18], tantalum oxide doped phosphate glass [9], zinc fluorophosphate glasses [19], boro-phosphate glasses [20], zinc-tungsten-antimonite glasses [21], titanium lead phosphate glasses [22], TeO_2− Lu_2O_3–WO_3 [23], etc., have been reported. Moreover, Zhao et al. [6] reported the heavy tellurite (70TeO_2–20ZnO − 10Lu_2O_3) doped with different Eu^{3+} concentrations for scintillation applications. Nandyala et al. [24] explored the time-resolved and PL performance of Eu^{3+} doped borosilicate (50B_2O_3–20SiO_2–20Na_2O–10CaO) glasses for display applications. Mariselvam et al. [25] studied spectral properties of Eu^{3+}-doped barium bismuth fluoroborate glasses.

In this present barium-bismuth-borate (Ba–Bi–B) glasses, Gd^{3+} ions act as sensitizer and Eu^{3+} ions act as acceptors. Gd^{3+} ions have a half-filled 4f shell with a stable ground state ($^8S_{7/2}$) and can be excited by ultra-violet (UV) light, and the accessible excitation states are ^6P_J, ^6I_J, and ^6D_J [10–12]. The energy transfer (ET) is the capability of energy interchange between the optically active ions. In recent years, ET made from Gd^{3+} to Eu^{3+} ions has been explored in several different glass hosts [26–31]. Yasutaka et al. [26] studied ET in Eu^{3+}-Gd^{3+} co-doped soda--lime silicate glasses and investigated time-resolved luminescence. Natalia et al. [27] reported the structural and optical properties of Eu^{3+}/Gd^{3+} ions in silica xerogels, Wantana et al. [28] investigated the energy transfer emission analysis of Eu^{3+} doped Gd_2O_3–CaO–SiO_2–B_2O_3 glasses for laser applications, Khan et al. [29] developed oxyfluoride glasses for efficient ET (Gd → Eu) to produce intense red emission for solid-state laser applications. Damdee et al. [30] studied Gd_2O_3 concentration on X-ray and photoluminescence properties of borate-based Eu-doped glasses for radiation detection materials and display device applications. Ramakrishna et al. [31] studied structural and radiative properties in Gd/Eu co-doped Li_2O–ZnO–SrO–B_2O_3–P_2O_5 glasses. Yue Zi et al. [8] deliberated heavy Eu^{3+}-doped boroalluminate (20Al_2O_3–60B_2O_3–(20–x) Gd_2O_3) glasses for x-ray detection applications.

Based on the review of literature, to obtain better characteristics for practical applications, the glass host as well as impurity concentration is crucial. The authors have been choosing new glass composition 45B_2O_3–15Bi_2O_3–30BaF_2–10TiO_2 with RE^{3+} (Eu^{3+}, and Gd^{3+}). Generally, borate glasses are one of the efficient luminescent materials with high thermal and chemical stability, and a high coefficient of combination of the RE ions [14,15]. The heavy metal oxides (HMO), bismuth oxide (Bi_2O_3), barium oxide (BaO), lead oxide (PbO), and titanium dioxide (TiO_2) are considered as intermediates in the glass matrices and are used for enhancing the optical properties via the formation of the glass structure [7,10,15]. The inclusion of TiO_2 in the glass systems can improve the linear refractive index and non-linear properties along with the thermal stability, chemical durability, and mechanical strength of the glasses [32,33]. Moreover, adding HMO leads to a decrease in the phonon energy and improves the luminescence properties of glass matrices [34,35]. The addition of barium fluoride (BaF_2) signifies the low phonon energy that causes less non-radiative (NR) relaxation rates and higher quantum efficiency of RE^{3+} in glass matrices [36,37].

In this direction, we investigated the structural and optical properties of Eu^{3+}-doped Ba–Bi–B glasses with different Gd_2O_3 compositions. The structural characteristics have been detailed by X-ray diffraction (XRD), Fourier-transform infrared spectroscopy (FTIR), and Raman spectroscopic studies. The Judd–Ofelt (J–O) [38,39] intensity parameters were evaluated and used to obtain radiative characteristics of the emission transition of Eu^{3+}-Gd^{3+} co-doped glasses. The ET mechanism from Gd^{3+} to Eu^{3+} ions by studying the behavior of PL profiles and time-resolved measurements of prepared glasses has been proposed.

2. Experimental details

The glass samples of the composition (44−x) B_2O_3–15Bi_2O_3–30BaF_2–10TiO_2–1Eu_2O_3–xGd_2O_3 (where x = 0, 0.5, 1.0, 2.0, 3.0, 4.0 and 5.0 mol%) were prepared by using melt quenching technique. All chemicals were mixed carefully and grounded to get the homogeneity of the powders and then placed in a high purity crucible (Al_2O_3) to be melted at 1050 °C for 1 h. Then the glass melt was quenched in air preheated brass plate and followed by annealing at 400 °C for 8 h. The glass samples were sliced and polished with a thickness of ~1.5 mm for further optical measurements. The samples are labeled according to the concentration of Gd_2O_3 and Eu^{3+} ions, as in Table 1. And also the optical photograph of all glasses (E0–E1G3.0) is presented in Fig. 1. All glass samples structure was investigated by powder XRD technique with Cu-K_α (monochromatic) radiation in the 2θ range 10–80 and NICOLET 20 FTIR spectrometer was used to record the FTIR spectra for all studied glasses. Raman spectra were measured by Lab Ram HR, Horiba, and Raman Spectrometer with ~785 nm as the excitation laser source. Optical absorption spectra were obtained using a Hitachi U-3900 UV–Vis spectrophotometer. The PL emission spectra, excitation spectra, and time-resolved spectroscopic measurements were recorded using an FLS 980 spectrofluorometer (Edinburgh Instruments, UK) equipped with a continuous wave Xenon lamp as a source and PMT as the detector.

3. Result and discussions

3.1. Physical characteristics

Calculations of physical factors, for instance, the average mol. weight ($Mol_{Avg.}$), density (ρ), molar volume (V_m), and oxygen packing density (OPD) for all studied glasses were performed based on the data of elemental composition and their respective values are presented in Table 2a (i) [40,41].

The density (ρ) values are found in the range of (4.253–4.421 g/cm^3), Mol_{Avg} (161.807–173.416 g/mol), V_m (38.225–39.226 cm^3/mol), are found to be increasing with increasing concentration of Gd^{3+} (0–3.0 mol%), while OPD values decrease (52.322–50.987 mol/lit) for all E0–E1G3.0 glasses. The concentrations of Eu^{3+} (1.567–1.535 × 10^{20} ions/cm^3), and Gd^{3+} (0–4.606 × 10^{20} ions/cm^3) were calculated for all E1–E1G3.0 glasses. The refractive index (n_d) values are found in the range of 1.739–1.749 for E0–E1G3.0 glasses. Molar refractivity values (15.400–15.965 cm^3) increase accordingly with the addition of RE ions, while it decreases the measure of metallization (0.597–0.593) for all E0–E1G3.0 glasses and as listed in Table 2a (i).

For all the cations (B^{3+}, Bi^{3+}, Ba^{2+}, Ti^{2+}, Eu^{3+}, and Gd^{3+}) in the glass composition, Pauling electronegativity (X_i), optical basicity moderating parameter (γ), and their optical basicity (Λ) values are presented in Table 2b (ii) [42]. The basicity values for E0–E1G3.0 glasses have been calculated by using the methods from earlier publications [43]. The Λ values are found in the range (0.448–0.465) for all studied glasses confirming the higher capability of oxide ions to donate electrons to surrounding cations.

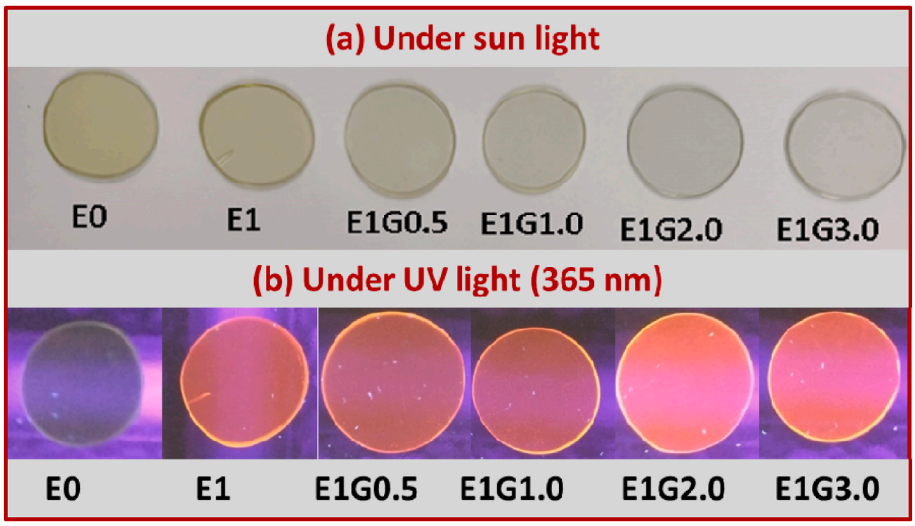

Fig. 1. (a) Graphical image of E0–E1G3.0 glasses (a) under sun light (b) under UV light (365 nm).

Table 2a
(i) Physical parameters of all (E0–E1G3.0) studied glasses.

Property	Glass Codes					
	E0	E1	E1G0.5	E1G1.0	E1G2.0	E1G3.0
Average Molecular Weight, g/mol	161.807	164.630	166.094	167.559	170.488	173.416
Density, ρ, g/cm^3	4.253	4.283	4.306	4.329	4.375	4.421
Eu^{3+} ion concentration, N_{Eu}^{3+} ($\times 10^{20}$ ions/cm^3)	0	1.567	1.561	1.556	1.545	1.535
Gd^{3+} ion concentration, N_{Gd}^{3+} ($\times 10^{20}$ ions/cm^3)	0	0	0.781	1.556	3.091	4.606
Refractive index, n_d	1.739	1.740	1.741	1.743	1.746	1.749
Dielectric constant, ε	3.024	3.028	3.031	3.038	3.049	3.059
Optical dielectric constant,	2.024	2.028	2.031	2.038	2.049	2.059
Molar volume, V_m, cm^3/mol	38.225	38.438	38.573	38.706	38.969	39.226
Oxygen packing density, OPD, mol/L	52.322	52.032	51.85	51.671	51.323	50.987
Molar Refractivity, R_m, cm^{-3}	15.400	15.502	15.572	15.658	15.812	15.965
Metallization criterion, M	0.597	0.597	0.596	0.596	0.595	0.593
Reflection loss, R_L, %	7.280	7.294	7.308	7.337	7.380	7.424
Molar Polarizability, α_m, cm^3 $\times 10^{-24}$	6.098	6.139	6.166	6.200	6.262	6.332
Glass optical basicity, Λ	0.448	0.452	0.454	0.457	0.461	0.465

Table 2b
(ii) Glass elements' optical basicity properties.

Cation	Electro negativity [X_i]	$\Lambda = (0.75/(X_i - 0.25)$	Oxides			Fluorides		
			Basicity moderating parameter γ	Oxide	$\Lambda = \gamma^{-1}$	Basicity moderating parameter	Fluoride	$\Lambda = \gamma^{-1}$
B^{3+}	2.04	0.4190	2.4208	B_2O_3	0.4131			
Bi^{3+}	2.02	0.4237	2.3936	Bi_2O_3	0.4178			
Ba^{2+}	0.89	1.1719	0.8568	BaO	1.1671	1.9706	BaF_2	0.5075
Ti^{2+}	1.54	0.5814	1.7408	TiO_2	0.5744			
Eu^{3+}	1.2	0.7895	1.2784	Eu_2O_3	0.7822			
Gd^{3+}	1.2	0.7895	1.2784	Gd_2O_3	0.7822			

3.2. X-ray diffraction analysis

The XRD profiles for all E0–E1G3.0 glasses have been presented in Fig. 2 (a). The XRD profiles do not show any crystalline peaks, while the broadly dispersed scattering was observed at lower angles at ~28°, confirming the present Ba–Bi–B glasses have amorphous nature only.

3.3. FTIR and Raman analysis

FTIR spectral studies are important to investigate the local structural and functional groups of the Eu − Gd co-doped Ba–Bi–B glasses. Fig. 2 (b) represents the FTIR spectra in absorbance mode and consisting of peaks at about 725, 877, 1053, 1248, 1390, 2897, 2975, and 3663 cm^{-1} for all E0–E1G3.0 glasses. All the bands' intensity was slightly increased with increasing of Gd^{3+} ions concentration in Eu-doped Ba–Bi–B glasses, and seems it did not cause any peak shift. Band positions at 2897, 2975, and 3663 are due to the O–H bond in the hydroxyl group [44]. The broadband in the range 920–1530 cm^{-1} consists of three bands; the band at 1053 cm^{-1} relates to the asymmetric stretching vibration modes of B–O, 1248 cm^{-1} is ascribed to the stretching mode of B–O bond in BO_4 units, and ~1390 cm^{-1} band has been attributed to the stretching of B–O bond in BO_3 units [45]. Also, a weak band at about 725 cm^{-1} is allocated to the B–O symmetrical bending vibration and 877 cm^{-1} is related to the stretching vibrations of di-borate B–O in BO_4 tetrahedra [44,45].

Fig. 2 (c) denotes the Raman spectra (200–3000 cm^{-1}) for all E0–E1G3.0 glasses and three bands can be seen in the spectra which are

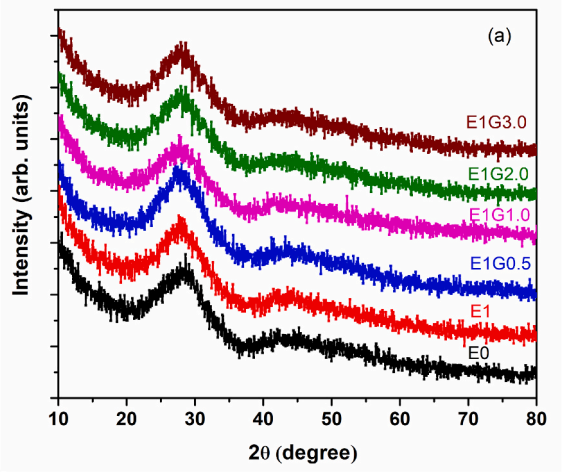

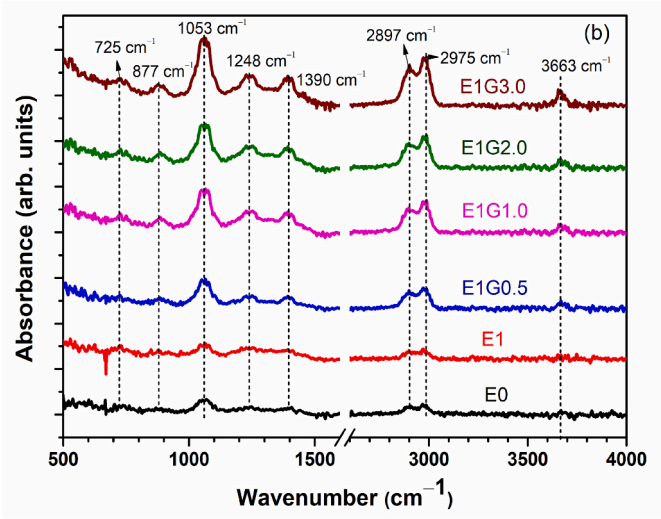

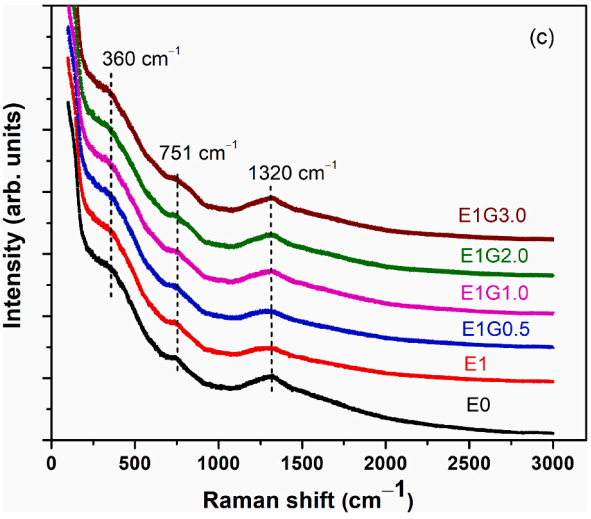

Fig. 2. (a) XRD analysis, (b) Infrared spectra, and (c) Raman spectra of E0–E1G3.0 glasses.

located at 360, 751, and 1320 cm^{-1}. The Raman study of Ba–Bi–B glasses revealed that Bi can form [BiO_3] pyramidal or [BiO_6] octahedral units. The band region from 240 to 670 cm^{-1} corresponds to the symmetric stretching mode in an angularly constrained Bi–O–Bi creation. The vibrations of Bi–O–Bi and [BiO_6] octahedral units appear at 360

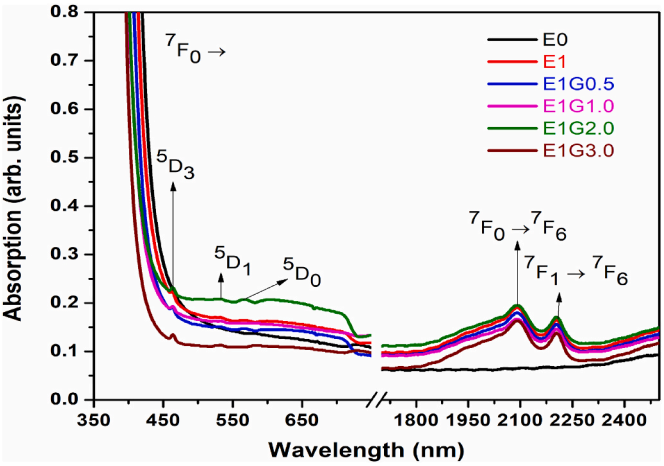

Fig. 3. Optical absorption spectrum UV–Vis–NIR regions for all E0–E1G3.0 glasses.

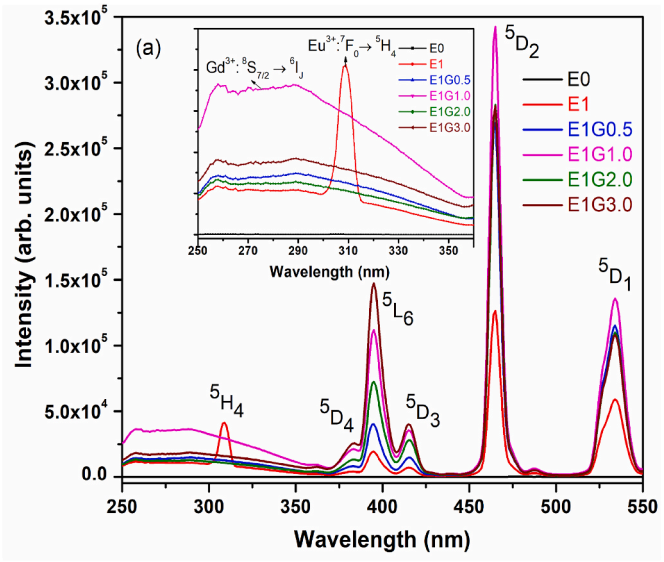

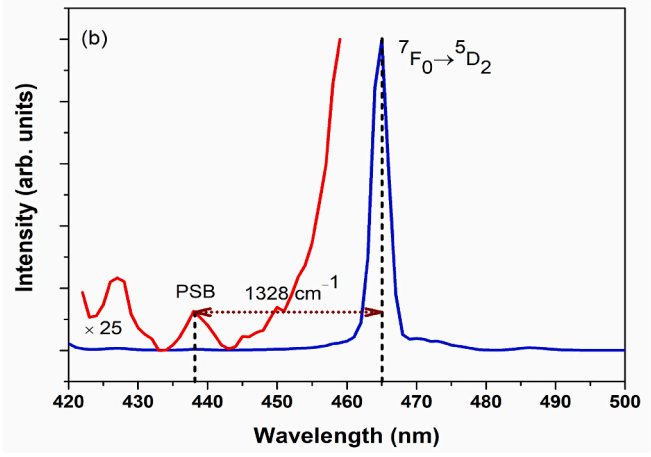

Fig. 4. (a) PL excitation spectra (250–550 nm) of Eu-Gd-doped Ba–Bi–B based glasses (b) Phonon side band (PSB) spectrum of Eu-doped Ba-Bi-B glasses.

cm^{-1} [46]. The Raman band (680–850 cm^{-1}) indicates the presence of BaO and TiO_2 and is related to the ring-type metaborate groups and loose BO_4 [44,47]. Furthermore, the Raman shift at 1320 cm^{-1} has the highest intensity compared with the remaining Raman bands of glasses

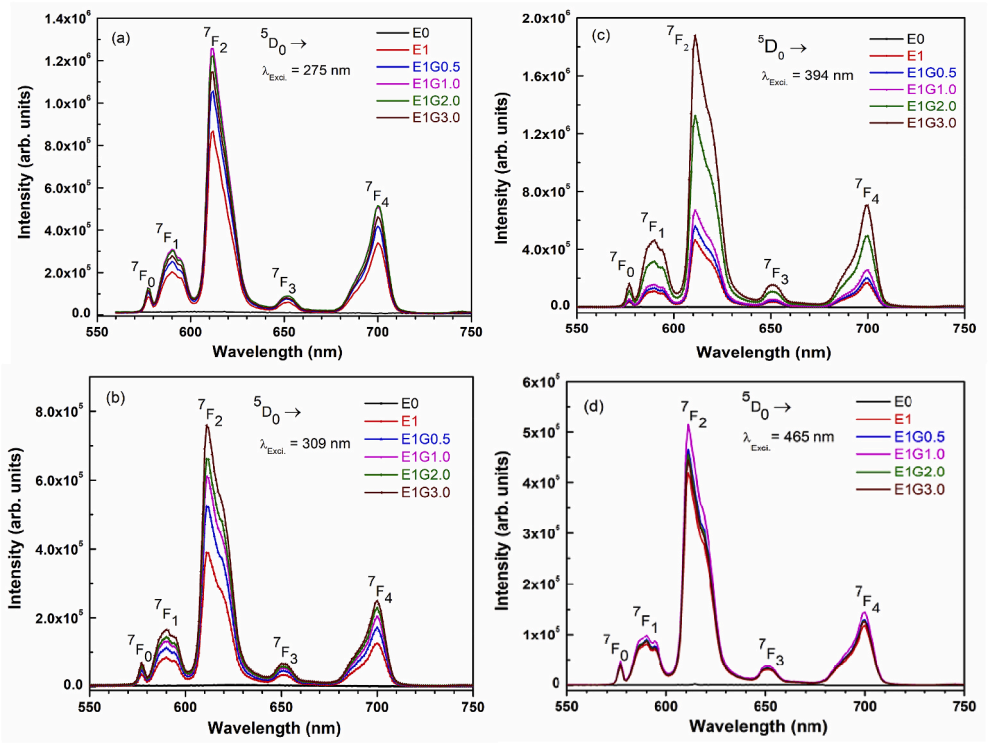

Fig. 5. Photoluminescence spectra E0–E1G3.0 glasses for different Gd concentrations under the excitation of different (a) $\lambda_{Exci.}$ = 275 nm (b) $\lambda_{Exci.}$ = 309 nm, (c) $\lambda_{Exci.}$ = 394 nm, (d) $\lambda_{Exci.}$ = 465 nm wavelengths.

and it can be attributed to the phonon energy of the studied glasses. From the excitation spectra of Eu-doped Ba–Bi–B glasses, phonon energy values were evaluated for their support.

3.4. Optical absorption and optical band gaps

Optical absorption spectra from 350 to 2500 nm of all E0–E1G3.0 glasses are presented in Fig. 3. The E0 spectrum has not shown any bands, but E1–E1G3.0 glasses have shown few optical bands in UV–Visible (350–750 nm) and MIR (1800–2500 nm) region. The absorption bands centered at 460 nm ($^7F_0 \rightarrow {}^5D_3$), 526 nm ($^7F_0 \rightarrow {}^5D_1$), 533 nm ($^7F_1 \rightarrow {}^5D_1$), 550 nm ($^7F_0 \rightarrow {}^5D_0$), 2095 nm ($^7F_0 \rightarrow {}^7F_6$), and 2186 nm ($^7F_1 \rightarrow {}^7F_0$), are attributed to the 4f-4f transitions of Eu^{3+} [7–9]. The cutoff wavelength position varies from 447 nm to 416 nm for E0–E1G3.0 glasses and is shown in Supplementary Fig. S1(a). The values are 447 nm (E0), 442 nm (E1), 434 nm (E1G0.5), 430 nm (E1G1.0), 422 nm (E1G2.0), and 416 nm (E1G3.0). The cutoff wavelength decreases with doping of Eu^{3+} ions and increasing Gd^{3+} concentration in the present glasses, indicating a decrease in non-bridging oxygen (NBOs) density in the studied glass system [24,26].

According to the previous report [48], optical bandgap values (E_{opt}) for E0–E1G3.0 glasses in direct band gap (E_{direct}) and indirect band gap ($E_{indirect}$) configurations were determined. All Tauc's plots [48] for E0–E1G3.0 glasses are presented in Fig. S1 (b) for direct band gap, and Fig. S1(c) for indirect band gap configurations, respectively. The band gap values are slightly increased in the range of (2.883–3.062 eV) for direct band gap and (2.756–2.939 eV) for indirect band gap configurations and these values have been presented and compared with the other reported values in Table S1 (supplementary). These values are comparable with ZSLBPEu (3.098 eV) [20], but are lower than KBZFB20 (3.87 eV) [17], ZFPEu (3.74 eV) [19], Eu1TiLP (3.58 eV) [22], Eu5TiLP (3.51 eV) [22], KTTBEu1 (3.235 eV) [49] glasses. An estimated E_{opt} value of E0–E1G3.0 glasses slightly increased due to the effect of Gd^{3+} ions concentration that causes the alternation of NBO density in the studied glasses.

Urbach energy (ΔE) is measured to be an amount of deficiencies in the glassy systems. The Urbach energy (ΔE) is evaluated from the inverse of the slope of ln (α) vs hν curves [50]. ΔE values are calculated for all E0–E1G3.0 glasses and found to be 0.148 eV (E0), 0.149 eV (E1), 0.151 eV (E1G0.5), 0.183 eV (E1G1.0), 0.144 eV (E1G2.0) and 0.126 eV (E1G3.0) see as in Fig. S1(d) (supplementary). These values are slightly increased with concentration (0–1 mol%) of Gd^{3+} ion and then decrease for E1G3.0 glasses. A slight variation ΔE value is usually expected as there is a chance of defect formation in the glass system. Sometimes these defect creations may lead to the deviation of optical bandgap values through an increase or decrease in the width of localized states that lie within the band gap [48]. The slighter variation in ΔE (0.148–0.183 eV) values of E0–E1G3.0 glasses confirms that these are free from such inadequacies in structure and the values are also comparable with reported KBZFB20 (0.33 eV) [17], KTTBEu1 (0.60 eV) [49] glasses.

3.5. PL excitation and phonon side band (PSB)

The PL excitation spectra of different concentrations of Gd^{3+} ions in Eu-doped Ba–Bi–B glasses monitored at $\lambda_{Emi.}$ = 612 nm are shown in Fig. 4 (a). The PL excitation peaks observed at 309, 360, 394, 420, 465, and 528 nm are ascribed to the Eu^{3+}: $^7F_0 \rightarrow {}^5H_4$, $^5D_4$, $^5L_6$, $^5D_3$, $^5D_2$, $^5D_1$ transitions, respectively in all E1–E1Gd3.0 glasses. The intensity of the most intense excitation band first increases with increasing Gd^{3+} concentration for 0–1.0 mol% and then decreases for 3.0 mol% of Gd^{3+} concentration. Additionally, a broad excitation band from 250 nm to 350 nm, corresponding to the Gd^{3+}: $^8S_{7/2} \rightarrow {}^6I_J$ transition was found in E1G0.5–E1G3.0 glasses. However, the excitation band of Eu^{3+}: $^7F_0 \rightarrow {}^5H_4$ transition (309 nm) was observed in E1 glasses, while it was not clearly observed for E1Gd0.5–E1Gd3.0 glasses. The absence of Eu^{3+}: $^7F_0 \rightarrow {}^5H_4$ band due to the ET from Gd^{3+}: $^6I_J \rightarrow {}^8S_{7/2}$ transition in Eu – Gd co-doped glasses. Gd^{3+} ions have an emission band at ~313 nm corresponding to the transition $^6I_J \rightarrow {}^8S_{7/2}$ [26,27]. The intensity of Eu^{3+}: $^7F_0 \rightarrow {}^5H_4$, $^5D_4$, $^5L_6$ transitions was increased with increasing

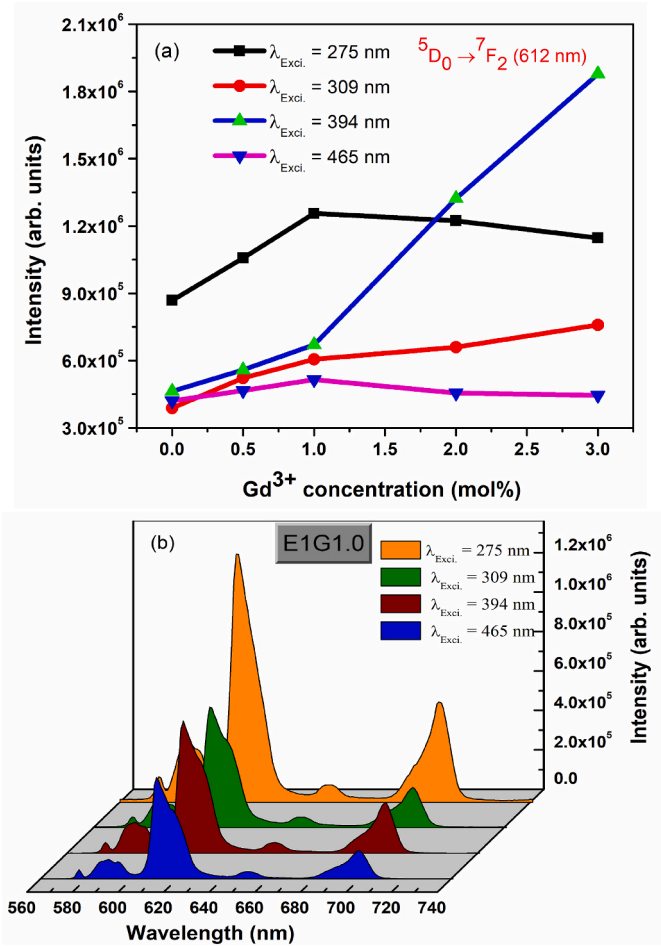

Fig. 6. (a) Variation of luminescence intensity (Eu^{3+}: $^5D_0 \rightarrow {}^7F_2$) with respect to Gd^{3+} concentration. (b) Emission spectra of E1G1.0 glasses under different excitation wavelengths.

Table 3
The Judd-Ofelt parameters (Ω_λ (λ = 2, 4, 6), × 10^{-20} cm^2) of Eu^{3+} -doped glass systems.

Composition	Ω_2 (× 10^{-20})	Ω_4 (× 10^{-20})	Ω_6 (× 10^{-20})
E1 (Present work)	5.13	4.86	–
E1G0.5 (Present work)	4.96	4.68	–
E1G1.0 (Present work)	5.13	4.78	–
E1G2.0 (Present work)	4.96	4.75	–
E1G3.0 (Present work)	4.61	4.44	–
$49.7NaPO_3$–$50Ta_2O_5$–$0.3Eu_2O_3$ [9]	4.58	3.82	–
KBZFB20 [17]	3.83	1.29	–
SBNCEu10 [18]	5.48	3.97	–
ZFPEu10 [19]	6.06	5.77	0.93
Eu1TiLP [22]	3.03	2.05	0.71
Eu5TiLP [22]	2.51	1.00	0.63
$40Li_2O$–5BaO – $5GdF_3$–$48SiO_2$–2.0Eu [29]	8.03	11.15	0.88
KTTBEu1 [49]	7.35	5.22	–
$75SiO_2$–$15Al_2O_3$–$10Na_2O$ –$1Eu_2O_3$ [54]	7.59	1.10	1.61
$62P_2O_5$–$32Li_2O$–$5Al_2O_3$–$1Eu_2O_3$ [55]	3.78	4.72	0.53
PKSAEu10 [56]	6.34	5.67	0.68

concentration of Gd^{3+} for 0–3.0 mol% in Eu-doped Ba–Bi–B glasses. While remaining bands Eu^{3+}: $^7F_0 \rightarrow {}^5D_3$, $^5D_2$, $^5D_1$ intensity was found to be maximum for Eu1G1.0 glasses and then decreases.

To calculate the phonon energy of the host glass and local structure around the Eu^{3+} in the glass matrix, the PSB spectrum can be used. Fig. 4 (b) displays the PSB centered at 22,830 cm^{-1} and located on the higher energy side of the pure electronic band (PEB) centered at 21,502 cm^{-1} (Eu^{3+}: $^7F_0 \rightarrow {}^5D_4$) for Ba–Bi–B glasses. The energy difference between PSB and PEB (zero phonon line) is 1328 cm^{-1} which happens to be the phonon energy of titled glass and is associated with the maximum energy of the vibrational mode coupled to the Eu^{3+} ions [50]. The estimated phonon energy value of 1328 cm^{-1} for Ba–Bi–B glasses and observed to the similar as that for $35Gd_2O_3$–$64B_2O_3$–$1Eu_2O_3$ glasses (1326 cm^{-1}), and less than $25Gd_2O_3$–$74B_2O_3$–$1Eu_2O_3$ for (1378 cm^{-1}) [30] but higher than $10K_2O$–10BaO–$10ZnF_2$–$68B_2O_3$ – $2Eu_2O_3$ (1300 cm^{-1}) [17], and 10CaO – $25Gd_2O_3$–$10SiO_2$–$55B_2O_3$–Eu_2O_3 (1274 cm^{-1}) [27] glasses. And finally, our results are comparable with the values of (PSB1: 970 cm^{-1} and PSB2: 1812 cm^{-1}) for LZSBP: Eu1 glasses [31]. The observed PSB (1328 cm^{-1}) is in good agreement with the intense broad Raman band around 1320 cm^{-1} in the Raman spectrum of the Ba–Bi–B glasses. It is well-known that the PSB band spectrum reflects the local vibrational environment and can directly estimate the phonon energy of the glass host material [51]. The phonon energy of the host lattice obstructs the radiative emission from excited states to the ground state through the NR process [33,34].

3.6. Emission and spectroscopic properties

Fig. 5(a–d) show emission spectra (550–750 nm) of Eu – Gd co-doped Ba–Bi–B glasses under 275, 309, 394, and 465 nm excitations. All emission profiles consist of five emission bands at 577, 591, 612, 651 and 700 nm corresponding to $^5D_0 \rightarrow {}^7F_0$, $^7F_1$, $^7F_2$, $^7F_3$ and $^7F_4$ transitions, respectively. Among these, the band at 612 nm due to the transition $^5D_0 \rightarrow {}^7F_2$ exhibited the most intense peak which is allowed by ED (electric dipole) and is sensitive to the local environment of Eu^{3+} ions. While MD (magnetic dipole) transition $^5D_0 \rightarrow {}^7F_1$ is not sensitive to the host local environment around Eu^{3+} ions drops in the sensible orange region [7–9]. The fluorescence intensity ratio (R) between $^5D_0 \rightarrow {}^7F_2$ (ED) and $^5D_0 \rightarrow {}^7F_1$ (MD) transitions is calculated for all E1–E1G3.0 glasses and these values are found to be 4.20, 4.19, 4.29, 4.19, 4.07 for E1, E1G0.5, E1G1.0, E1G2.0, and E1G3.0 glasses, respectively. This value tells the degree of chemical bonding of Eu^{3+} ions and the nature of covalency of the Eu–O band. The higher values (R = 4.07–4.20) specify the higher asymmetry and stronger covalency around the Eu^{3+} ion for studied glasses [22].

Fig. 6 (a) shows the trending emission intensity profiles of the transition $^5D_0 \rightarrow {}^7F_2$ (~612 nm) under the different excitation wavelengths 275 nm, 309 nm, 394 nm, and 465 nm for different concentrations of Gd^{3+} ions in studied glasses. All transitions intensity profiles follow the same trend and the peak increased from E0 →E1G3.0 glasses 309 nm, and 394 nm excitations, while under 275 nm and 465 nm excitations, the PL emission intensity increases from Eu0 to Eu1G1.0 and then decreases with increasing Gd^{3+} ion concentration to 3.0 mol%. During the excitation processes for obtaining emission bands, the concentration of doping ions (i.e., Eu^{3+} and Gd^{3+}) and excitation sources were playing a crucial role, and also various channels i.e., non-radiative (NR), cross-relaxation (CR), and energy transfer (ET) are influenced under the de-excitation process [29–31].

Fig. 6(b) represents the emission spectra of E1G1.0 glasses under 275 nm, 309 nm, 394 nm, and 465 nm excitations, and observed emission intensity profiles varied accordingly with a variation of excitation bands wavelengths [see excitation spectra Fig. 4 (a)]; however, there was no any noticeable peak shifting in emission profiles.

J–O theory [38,39] provides information about the local environment and bonding in the proximity of the RE^{3+} ions by evaluating the (J–O) intensity parameters, Ω_J (J = 2, 4, 6). Ω_2 is interrelated to the covalency and structural changes in the chemical environment of ligand ions of the RE^{3+} ion and parameter Ω_4 extends the host matrix rigidity [52]. J–O intensity parameters calculations and their related procedure were detailed by Werts et al. [53] and other researchers [49,54–56]. Intensity parameters Ω_J (J = 2, 4, 6) were evaluated using the PL spectra

Table 4
Emission peak positions (λ_p, nm), effective bandwidths ($\Delta\lambda_{eff}$, nm), radiative transition probabilities (A_R, S^{-1}), stimulated emission cross-section (σ_{emi}, $\times 10^{-21}$ cm^2), gain bandwidth parameter ($\sigma_{emi} \times \Delta\lambda_{eff}$) ($\times 10^{-26}$ cm^3), experimental (β_{exp}) and calculated (β_{cal}) branching ratios, total radiative transition probability (A_T, s^{-1}) and radiative lifetime (τ_R, μs) for all E1–E1G3.0 glasses.

Glasses	Transitions $^5D_0 \rightarrow$	λ_p	$\Delta\lambda_{eff}$	A_R	σ_{emi}	$\sigma_{emi} \times \Delta\lambda_{eff}$	β_{exp}	β_{cal}	A_T	T_{rad}
E1 (Present work)	$^7F_0$	577	11.75	0.000	0	0	0.03	0.000	452.313	2210
	$^7F_1$	591	12.02	75.01	0.3360	403.87	0.15	0.166		
	$^7F_2$	612	16.03	255.58	0.9806	1571.9	0.54	0.565		
	$^7F_3$	651	15.26	0.00	0.00	0.0	0.04	0.000		
	$^7F_4$	700	15.37	121.72	0.8384	1288.6	0.24	0.269		
E1G0.5 (Present work)	$^7F_0$	578	9.92	0.000	0.0	0.0	0.02	0.000	440.897	2268
	$^7F_1$	591	15.96	75.13	0.2531	403.95	0.16	0.170		
	$^7F_2$	612	16.17	248.57	0.9439	1526.29	0.54	0.564		
	$^7F_3$	652	14.50	0.00	0.000	0.0	0.04	0.000		
	$^7F_4$	700	13.13	117.20	0.9436	1238.95	0.24	0.266		
E1G1.0 (Present work)	$^7F_0$	578	13.38	0.000	0.0	0.0	0.03	0.000	453.916	2203
	$^7F_1$	591	15.15	75.39	0.2671	404.66	0.15	0.166		
	$^7F_2$	612	15.60	258.10	1.0141	1582.0	0.54	0.569		
	$^7F_3$	652	16.03	0.000	0.000	0.0	0.04	0.000		
	$^7F_4$	700	14.05	120.43	0.9038	1269.0	0.24	0.265		
E1G2.0 (Present work)	$^7F_0$	578	12.97	0.000	0.00	0.0	0.03	0.000	448.633	2228
	$^7F_1$	591	16.60	76.04	0.2444	405.70	0.16	0.170		
	$^7F_2$	612	16.26	252.00	0.9440	1534.94	0.53	0.562		
	$^7F_3$	652	15.72	0.000	0.000	0.0	0.04	0.000		
	$^7F_4$	700	11.92	120.59	1.0612	1264.95	0.24	0.269		
E1G3.0 (Present work)	$^7F_0$	578	13.74	0.000	0	0.0	0.03	0.000	426.209	2346
	$^7F_1$	591	15.70	76.57	0.2590	406.63	0.16	0.180		
	$^7F_2$	612	14.11	236.05	1.0147	1431.74	0.52	0.554		
	$^7F_3$	652	22.89	0.00	0.00	0.00	0.05	0.000		
	$^7F_4$	700	14.36	113.59	0.8257	1185.71	0.24	0.267		

Table 5
Comparison of spectroscopic parameters emission peak positions (λ_p, nm), effective bandwidths ($\Delta\lambda_{eff}$, nm), radiative transition probabilities (A_R, S^{-1}), stimulated emission cross-section (σ_{emi}, $\times 10^{-21}$ cm^2), gain bandwidth parameter ($\sigma_{emi} \times \Delta\lambda_{eff}$) ($\times 10^{-26}$ cm^3), experimental (β_{exp}) and calculated (β_{cal}) branching ratios, and radiative lifetime (τ_R, ms) of transitions ($^5D_0 \rightarrow ^7F_2$) for all E1–E1G3.0 glasses.

Glasses	λ_p (nm)	$\Delta\lambda_{eff}$ (nm)	A_R (S^{-1})	σ_{emi} ($\times 10^{-21}$ cm^2)	$\sigma_{emi} \times \Delta\lambda_{eff}$ ($\times 10^{-26}$ cm^3)	β_{exp}	β_{cal}	τ_R ms
E1 (Present work)	612	16.03	255.58	0.9806	1571.9	0.54	0.56	2.210
E1G0.5 (Present work)	612	16.17	248.57	0.9439	1526.29	0.54	0.56	2.268
E1G1.0 (Present work)	612	15.60	258.10	1.0141	1582.0	0.54	0.57	2.203
E1G2.0 (Present work)	612	16.26	252.00	0.9440	1534.94	0.53	0.56	2.228
E1G3.0 (Present work)	612	14.11	236.05	1.0147	1431.74	0.52	0.55	2.346
KBZFB20 [17]	612	10.13	–	0.95	962.35	0.63	–	2.800
SBNCEu [18]	612	11.48	230.6	1.056	1212.29	0.54	0.61	2.640
ZFPEu10 [19]	611	10.0	203.0	1.58	1580	0.66	0.58	2.830
Boro-phosphate [20]	615	3.22	191.44	1.933	622.43	0.69	–	3.640
2Eu ZSLBP [20]	615	3.89	219.73	2.012	782.67	0.74	–	3.388
Eu1TiLP [22]	611	12.65	–	0.740	936.10	0.56	0.55	3.704
Eu5TiLP [22]	611	12.51	–	0.631	789.38	0.56	0.57	4.347
$10CaO–25Gd_2O_3–10SiO_2–54.70B_2O_3–0.30Eu_2O_3$ [28]	614	–	779.42	3.751	–	0.68	0.67	–
KTTBEu1 [49]	613	5.57	330.70	0.728	405.50	0.64	0.63	1.910
$62P_2O_5–32Li_2O–5Al_2O_3–1Eu_2O_3$ [55]	612	11.16	159	0.86	959.76	0.61	0.63	–
PKSAEu10 [56]	609	10.36	187	1.280	1326.08	0.69	0.75	2.87

and refractive index of glass materials. Ω_2 and Ω_4 parameters were estimated for Eu^{3+} and Eu − Gd co-doped Ba–Bi–B glasses and their values are presented in Table 3. And the standard deviation (‘σ ‘) values are found to be 0.21 and 0.16 $\times 10^{-20}$ cm^2 for Ω_2 and Ω_4 parameters, respectively. The calculated intensity parameter values are comparable with the other reported results [9,17–19,22,29,49,54–56]. Ω_2 and Ω_4 values are found to be in the range 5.13–4.61 $\times 10^{-20}$ cm^2 and 4.86–4.44 $\times 10^{-20}$ cm^2 for E1–E1G3.0 glasses. As seen from Table 3, $\Omega_2 = 5.13 \times 10^{-20}$ cm^2 and $\Omega_4 = 4.78 \times 10^{-20}$ cm^2 for E1G1.0 are smaller than that of ZFPEu10 ($\Omega_2 = 6.06 \times 10^{-20}$ cm^2 and $\Omega_4 = 5.77 \times 10^{-20}$ cm^2) [19], KTTBEu1 ($\Omega_2 = 7.35 \times 10^{-20}$ cm^2 and $\Omega_4 = 5.22 \times 10^{-20}$ cm^2) [49], $10Na_2O–15Al_2O_3–75SiO_2–1Eu_2O_3$ ($\Omega_2 = 7.59 \times 10^{-20}$ cm^2) [54], $40Li_2O–5BaO – 5GdF_3–48SiO_2–2.0Eu$ ($\Omega_2 = 8.03 \times 10^{-20}$ cm^2 and $\Omega_4 = 11.15 \times 10^{-20}$ cm^2) [29] and PKSAEu10 ($\Omega_2 = 6.34 \times 10^{-20}$ cm^2 and $\Omega_4 = 5.67 \times 10^{-20}$ cm^2) [56] glass systems but are higher than that of the $49.7NaPO_3–50Ta_2O_5–0.3Eu_2O_3$ ($\Omega_2 = 4.58 \times 10^{-20}$ cm^2 and $\Omega_4 = 3.82 \times 10^{-20}$ cm^2) [9], KBZFB20 ($\Omega_2 = 3.83 \times 10^{-20}$ cm^2 and $\Omega_4 = 1.29 \times 10^{-20}$ cm^2) [17], Eu1TiLP ($\Omega_2 = 3.03 \times 10^{-20}$ cm^2 and $\Omega_4 = 2.05 \times 10^{-20}$ cm^2) [22], Eu5TiLP ($\Omega_2 = 2.51 \times 10^{-20}$ cm^2 and $\Omega_4 = 1.00 \times 10^{-20}$ cm^2) [22], $62P_2O_5–32Li_2O–5Al_2O_3–1Eu_2O_3$ ($\Omega_2 = 3.78 \times 10^{-20}$ cm^2 and $\Omega_4 = 4.72 \times 10^{-20}$ cm^2) [55] and SBNCEu10 ($\Omega_2 = 5.48 \times 10^{-20}$ cm^2 and $\Omega_4 = 3.97 \times 10^{-20}$ cm^2) [18] glass systems (see Table 3).

Radiative factors are very essential to estimate the laser transition features to evaluate performance in laser display devices. J–O intensity values are used to govern the radiative parameters for all studied glasses and have been calculated by using the relations from previous reports [13–16,57]. Table 4 represents the spectroscopic characteristics i.e., emission peak positions (λ_p, nm), effective bandwidths ($\Delta\lambda_{eff}$, nm), radiative transition probabilities (A_R, S^{-1}), stimulated emission cross-section (σ_{emi}, $\times 10^{-21}$ cm^2), gain bandwidth parameter ($\sigma_{emi} \times \Delta\lambda_{eff}$) ($\times 10^{-26}$ cm^3), experimental (β_{exp}) and calculated (β_{cal}) branching ratios, total radiative transition probability (A_T, s^{-1}) and radiative lifetime (τ_R, μs) for the present study of Gd^{3+} influence in Eu-doped Ba–Bi–B glasses. Intense emission transition $^5D_0 \rightarrow ^7F_2$ (612 nm) was

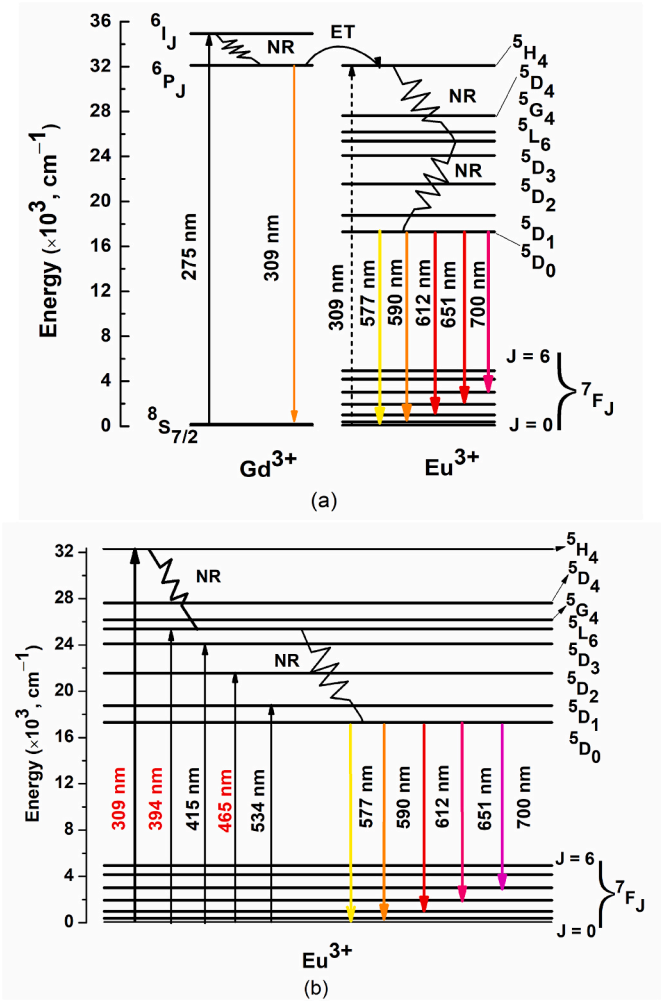

Fig. 7. (a) Energy Level Diagram of Gd^{3+} and Eu^{3+} ions in Ba–Bi–B glasses. (b) Energy Level Diagram of Eu^{3+} ions in Ba-Bi-B glasses.

observed in all E1–E1G3.0 glasses and possesses higher $\beta_{exp} = 0.54$, $A_R = 258.10\ s^{-1}$, $\sigma_{emi} = 1.01 \times 10^{-21}\ cm^2$, gain bandwidth parameter $\sigma_{emi} \times \Delta\lambda_{eff} = 1582.0$, $A_T = 453.916\ s^{-1}$, radiative lifetime $\tau_R = 2203\ \mu s$ for E1G1.0 glass (see Table 4).

Spectral characteristics of all studied Ba–Bi–B glasses were compared with different composition of Eu^{3+} and Eu^{3+}-Gd^{3+} doped materials in Table 5 [17–20,22,28,49,55,56]. As seen from Table 5, $\sigma_{emi} = 1.01 \times 10^{-21}\ cm^2$ (E1G1.0) value is comparable with KBZFB20 ($\sigma_{emi} = 0.95 \times 10^{-21}\ cm^2$) [17], SBNCEu ($\sigma_{emi} = 1.056 \times 10^{-21}\ cm^2$) [18], and PKSAEu10 ($\sigma_{emi} = 1.280 \times 10^{-21}\ cm^2$) [56], while it higher than that for Eu1TiLP ($\sigma_{emi} = 0.740 \times 10^{-21}\ cm^2$) [22], Eu5TiLP ($\sigma_{emi} = 0.631 \times 10^{-21}\ cm^2$) [22], KTTBEu1 ($\sigma_{emi} = 0.728 \times 10^{-21}\ cm^2$) [49], $62P_2O_5$–$32Li_2O$–$5Al_2O_3$–$1Eu_2O_3$ ($\sigma_{emi} = 0.86 \times 10^{-21}\ cm^2$) [55] glass systems, but it slower than ZFPEu10 ($\sigma_{emi} = 1.58 \times 10^{-21}\ cm^2$) [19], Boro-phosphate ($\sigma_{emi} = 1.933 \times 10^{-21}\ cm^2$), 2EuZSLBP ($\sigma_{emi} = 2.012 \times 10^{-21}\ cm^2$) [20], and $10CaO - 25Gd_2O_3$–$10SiO_2$–$54.70B_2O_3$–$0.30Eu_2O_3$ ($\sigma_{emi} = 3.751 \times 10^{-21}\ cm^2$) [28] glass systems.

3.7. Energy transfer and energy level diagram

The possibility of ET between Eu^{3+} and Gd^{3+} ions was demonstrated in the energy level diagram of Eu^{3+} and Gd^{3+} ions co-doped Ba–Bi–B glasses, as shown in Fig. 7(a). According to the energy level diagram in Fig. 7 (a), under 275 nm excitation, the photons are absorbed by Gd^{3+} ions from the $^8S_{7/2}$ (ground state) to ^6I_J excited state of 4 F^7–4 F^7 intra configurational transitions. The excited electrons in Gd^{3+} relax down to ^6P_J (Gd^{3+}) state, and then transfer energy non-radiatively (NR) as a sensitizer to the Eu^{3+} ion in the effect of the ^6I_J (Gd^{3+}) → $^5H_4$ (Eu^{3+}) transition as first process [28,29] and in addition, the Gd^{3+} ions also radiatively relax to the ground state Gd^{3+}: $^8S_{7/2}$ with broad emission from band in 290–340 nm. Meanwhile, the strong absorption of Eu^{3+} ions ($^7F_0 \rightarrow {}^5H_4$) was observed from an excitation spectrum of 1mol% Eu ions in Ba–Bi–B glasses, which is depicted in Fig. 7 (a) by the dotted upward arrow. So, energy transfer occurred between $Gd^{3+} \rightarrow Eu^{3+}$ ions, owing to the equal energy levels of Gd^{3+} emission and Eu^{3+} excitation peak at ~309 nm as a second process. Through both energy transfer processes, excited electrons reach Eu^{3+}: $^5H_4$ and then through NR relaxation to the $^5D_0$ transition. Finally, the photons are emitted via the radiative transitions to different states Eu^{3+}: $^7F_0$, $^7F_1$, $^7F_2$, $^7F_3$, and $^7F_4$, and give rise to the visible emission peaks at 577, 590, 612, 651, and 700 nm, respectively.

Fig. 7(b) depicts the partial energy level diagram of Eu^{3+} ions and it does confirm the possible excitation and emissions transitions in the present study. And also, illustrates the potential PL emission transitions by different excitation wavelengths ($\lambda_{Exci.} = 309$, 394, and 465 nm). The excited photons reach their respective excitation levels and then drop to the $^5D_0$ transition via the NR process as shown in Fig. 7 (b). Due to a large energy gap between the $^5D_0$ state (17,301 cm^{-1}) and the next lower-lying $^7F_6$ level (4924 cm^{-1}) [57,58], the representative emission lines can be observed Eu^{3+}: $^5D_0 \rightarrow {}^7F_J$ (i.e., $^7F_0$, $^7F_1$, $^7F_2$, $^7F_3$, and $^7F_4$ transitions) and are attributed to the 577, 590, 612, 651, and 700 nm, respectively. Under the various excitation wavelengths, the emission lines peaked at the same position, but the intensity was varied according to the alteration of concentration of Eu^{3+} and Gd^{3+} ions, energy transfer ($Gd^{3+} \rightarrow Eu^{3+}$) and NR channels in the de-excitation process [29–31,56,59]. These results were confirmed from emission spectral profiles of studied glasses at different excitation wavelengths and also obtain strong evidence from the lifetime values of present samples.

3.8. Luminescence decay analysis at different excitation wavelengths

Decay curve analysis helped to investigate the metastable lifetime values of Eu^{3+} ions and calculate the photons during the de-excitation process of Eu^{3+} ions in Ba–Bi–B glasses. The PL decay curves of the most intense emission peak at 612 nm of E1–E1G3.0 co-doped Ba–Bi–B glasses excited by different excitation wavelength $\lambda_{Exci.} = 275$, 309, 394, and 465 nm are depicted Fig. 8(a–d). All the decay profiles were fitted to the double non-exponential decay described by the following relation:

$$I(t) = B_0 + B_1 \exp(-t/\tau_1) + B_2 \exp(-t/\tau_2) \quad (1)$$

where B_0, B_1, and B_2 are constants obtained from the curve fitting, t = time, and τ_1, and τ_2 are decay time values for exponential components, respectively.

All decay curves exhibited non-exponential natures and lifetime values were calculated using the following expressions [19].

$$\tau_{exp} = \frac{B_1\tau_1^2 + B_2\tau_2^2}{B_1\tau_1 + B_2\tau_2} \quad (2)$$

All the individual lifetime values (τ_{exp}) for transition $^5D_0 \rightarrow {}^7F_2$ (612 nm) of E1–E1G3.0 glasses at different excitation wavelengths are presented in Table 6a. τ_{exp} values are found to slightly rises with increasing Gd^{3+} ion concentration from 0 to 1.0 mol% and then decreases in co-doped glasses in all different excitation wavelengths. It's due to the stronger interactions including the NR process and cross-relaxation (CR) could be responsible for the excitation energy loss or migration in Eu^{3+} ions. In co-doped (Eu^{3+}/Gd^{3+}) systems energy transfer processes should be more responsible for the differences in lifetime values [29–31]. The effect of Gd^{3+} ions concentration on lifetime values and different excitation conditions are presented in Fig. 9.

Among all samples E1G1.0 sample holds the highest τ values of 1.353 ms ($\lambda_{Exci.} = 275$), 1.377 ms ($\lambda_{Exci.} = 309$), 1.583 ms ($\lambda_{Exci.} = 394$),

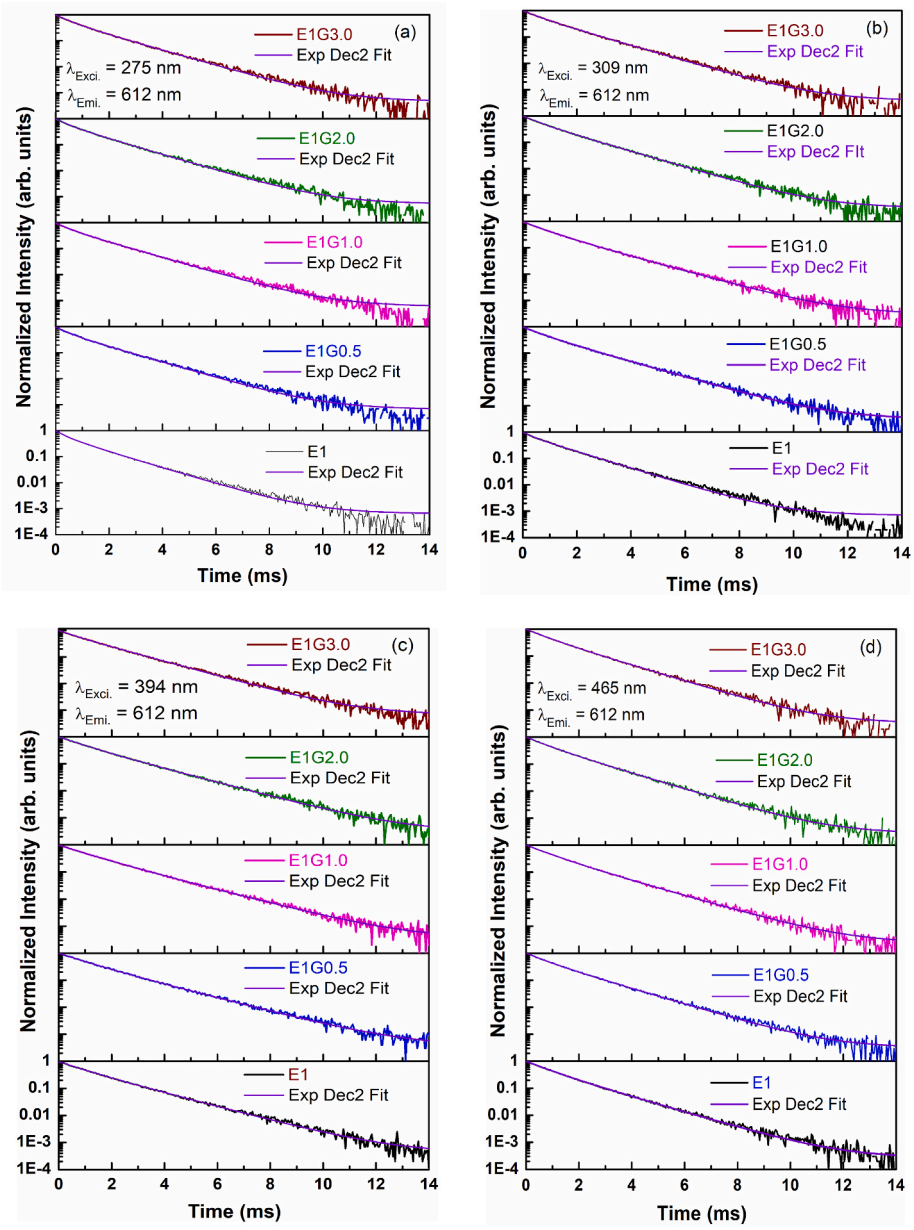

Fig. 8. Photoluminescence decay profiles under different excitation (a) 275 nm (b) 309 nm (c) 394 nm and (d) 465 nm of $^5D_0 \rightarrow {}^7F_2$ transition for E1–E1G3.0 glasses.

Table 6a
(i) Lifetime values of Eu^{3+}: $^5D_0 \rightarrow {}^7F_2$ under different excitation wavelengths for E1–E1G3.0 glasses.

Glass Label	$^5D_0 \rightarrow {}^7F_2$ (τ, μs) λ_{exc} = 275 nm λ_{emi} = 612 nm	$^5D_0 \rightarrow {}^7F_2$ (τ, μs) λ_{exc} = 309 nm λ_{emi} = 612 nm	$^5D_0 \rightarrow {}^7F_2$ (τ, μs) λ_{exc} = 394 nm λ_{emi} = 612 nm	$^5D_0 \rightarrow {}^7F_2$ (τ, μs) λ_{exc} = 465 nm λ_{emi} = 612 nm
E1	1.272	1.305	1.569	1.369
E1G0.5	1.333	1.357	1.580	1.370
E1G1.0	1.353	1.377	1.583	1.378
E1G2.0	1.328	1.350	1.543	1.338
E1G3.0	1.315	1.329	1.536	1.343

and 1.378 ms ($\lambda_{Exci.}$ = 275), due to the maximum ET from Gd^{3+} to Eu^{3+} ions. Meanwhile, τ values are found to be maximum of 1.569 ms (E1), 1.580 ms (E1G0.5), 1.583 ms (E1G1.0), 1.543 ms (E1G2.0), and 1.536 ms (E1G3.0) for transition $^5D_0 \rightarrow {}^7F_2$ at $\lambda_{Exci.}$ = 394 nm. The τ_{exp}, τ_R, and quantum efficiency (η) values are evaluated for all E1G1.0 Ba–Bi–B glasses and tabulated and also compared in Table 6b. As seen from Table 6b, quantum efficiency η = 0.72 for E1G1.0 is lower than SBNCEu10 (0.91) [18], ZFPEu10 (0.87) [19], 1EuKTTB (0.86), and higher than $49.7NaPO_3$–$50Ta_2O_5$–$0.3Eu_2O_3$ (0.55 ms) [9], Eu1TiLP (0.632) [22], Eu5TiLP (0.544) [22], and PKSAEu10 (0.63) [56] glass systems.

3.9. CIE color coordinates and CCT analysis

Commission Internationale de l'Eclairage (CIE) chromaticity coordinates of the luminescence characteristics are estimated according to the expressions from previous reports [60,61]. CIE coordinates values are evaluated from the PL emission spectra of all the samples for different excitation wavelengths in Eu^{3+}–Gd^{3+} co-doped Ba–Bi–B glasses and the results are presented in Table 7. CIE coordinates are found to be similar: (676, 0.323) at λ_{exci} = 275 nm; (664, 0.335) at λ_{exci} = 309 nm; (662, 0.337) at λ_{exci} = 394 nm; (665, 0.335) at λ_{exci} = 465 nm, for all E1–E1G3.0 glasses and are shown in 1931 chromaticity

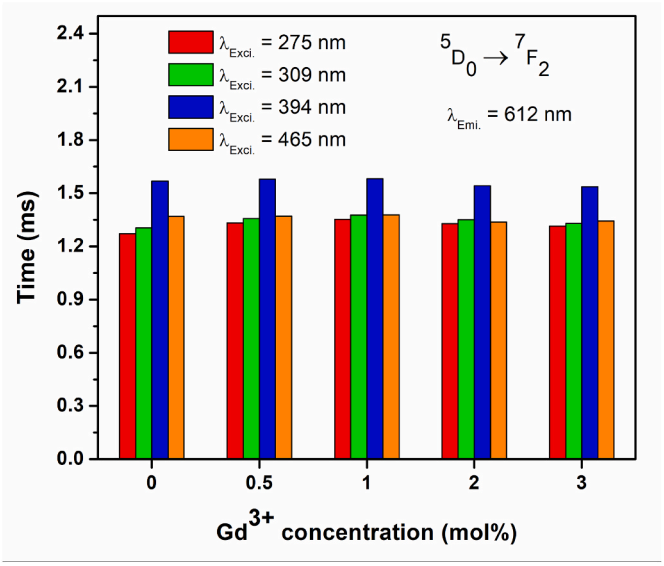

Fig. 9. Bar diagram of decay values at under different excitation source ($\lambda_{exci.}$ = 275 nm, 309 nm, 394 nm and 465 nm) of $^5D_0 \rightarrow {}^7F_2$ transition for E1–E1G3.0 glasses.

Table 6b
(ii) Lifetime values of Eu^{3+}: $^5D_0 \rightarrow {}^7F_2$ transition (λ_{exc} = 393 nm, λ_{emi} = 612 nm) and energy transfer efficiency for all E1–E1G3.0 glasses.

Glass Label	$^5D_0 \rightarrow {}^7F_2$($\tau_{exp}$, μs) λ_{exc} = 394 nm λ_{emi} = 612 nm	$^5D_0 \rightarrow {}^7F_2$ (τ_R, μs)	Energy transfer efficiency ($\eta = \tau_{exp}/\tau_R$)
E1 (Present work)	1.569	2.210	0.71
E1G0.5 (Present work)	1.580	2.268	0.70
E1G1.0 (Present work)	1.583	2.203	0.72
E1G2.0 (Present work)	1.543	2.228	0.69
E1G3.0 (Present work)	1.536	2.346	0.65
49.7$NaPO_3$–50Ta_2O_5–0.3Eu_2O_3 [9]	0.940	1.690	0.55
SBNCEu10 [18]	2.416	2.640	0.91
ZFPEu10 [19]	2.47	2.830	0.87
Eu1TiLP [22]	2.341	3.704	0.63
Eu5TiLP [22]	2.365	4.347	0.54
KTTBEu1 [49]	1.65	1.91	0.86
PKSAEu10 [56]	2.50	3.99	0.63

diagram (Fig. 10).

Correlated color temperature (CCT) values are also derived using McCamy's approximate equation [61,62]:

$$CCT = -449n^3 + 3525n^2 - 6823.3n + 5520.33 \quad (3)$$

where, $n = (x - x_e)/(y - y_e)$ is the inverse slope; $x_e = 0.332$ and $y_e = 0.186$ are the epicenter of convergence. CCT values are evaluated for all PL spectra at different excitation wavelengths and are presented in Table 7. CIE coordinates and CCT values of all studied glasses show no any influence of concentration of Gd^{3+} ions, however different excitation wavelengths alter the CIE and CCT values: 3504K (λ_{exci} = 275 nm), 2851K (λ_{exci} = 309 nm), 2758K (λ_{exci} = 394 nm), and 2865K (λ_{exci} = 465 nm) for all E1–E1G3.0 glasses. The CCT values range (3505 K–2758 K) indicates the warms colors category and the glasses are suitable for display device applications. All the CIE coordinates lay in the red spectral region due to the most dominant Eu^{3+}: $^5D_0 \rightarrow {}^7F_2$ (612 nm) transition among all the PL band and this transition can be suitable in the field of laser display devices.

Table 7
CIE color coordinates (x, y) and CCT (K) values under different excitation wavelengths of PL spectra for all E1–E1G3.0 glasses.

Glass label	Parameters	Excitation wavelengths			
		275 nm	309 nm	393 nm	465 nm
E1	(x, y)	(0.676, 0.323)	(0.664, 0.335)	(0.662, 0.337)	(0.665, 0.335)
	CCT (K)	3504	2851	2758	2865
E1G0.5	(x, y)	(0.676, 0.323)	(0.664, 0.335)	(0.662, 0.337)	(0.665, 0.335)
	CCT (K)	3504	2851	2758	2865
E1G1.0	(x, y)	(0.676, 0.323)	(0.664, 0.335)	(0.662, 0.337)	(0.665, 0.335)
	CCT (K)	3504	2851	2758	2865
E1G2.0	(x, y)	(0.676, 0.323)	(0.664, 0.335)	(0.662, 0.337)	(0.665, 0.335)
	CCT (K)	3504	2851	2758	2865
E1G3.0	(x, y)	(0.676, 0.323)	(0.664, 0.335)	(0.662, 0.337)	(0.665, 0.335)
	CCT (K)	3504	2851	2758	2865

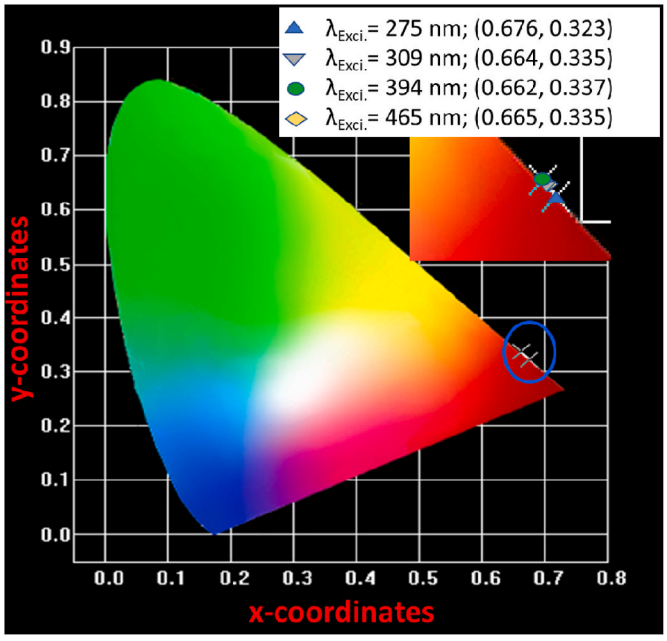

Fig. 10. CIE plots of Eu-Gd-doped Ba–Bi–B based glasses.

4. Conclusions

In summary, structural, PL, and time-resolved activities of Eu^{3+}–Gd^{3+} co-doped Ba–Bi–B glasses were investigated. XRD results of the powder sample reveal the non-crystalline nature of the studied glasses. Optical band gaps were evaluated in direct (2.883–3.062 eV), and indirect (2.756–2.939 eV) configurations for all E1–E1G3.0 glasses. The band gaps were found to increase with increasing Gd^{3+} ions concentration (0–3.0 mol%) of the glasses under investigation.

J-O parameters are found in range $\Omega_2 = 5.13–4.61 \times 10^{-20}$ cm^2 and $\Omega_4 = 4.86–4.44 \times 10^{-20}$ cm^2 for all E1–E1G3.0 glasses. Under UV excitation (275 nm), an efficient $Gd^{3+} \rightarrow Eu^{3+}$ energy transfer process was observed that enhanced the luminescence of Eu^{3+} ions. Gd^{3+} ions concentration (1.0 mol %) was optimized for getting an intense prominent red emission ~612 nm (Eu^{3+}: $^5D_0 \rightarrow {}^7F_2$) in E1–E1G3.0 glasses. The optimized glass (E1G1.0) has the efficient spectroscopic characteristics; $\Delta\lambda_{eff}$ = 15.60 nm, A_R = 258.10 S^{-1}, $\sigma_{emi} = 10.14 \times 10^{-22}$ cm^2, gain bandwidth parameter $\sigma_{emi} \times \Delta\lambda_{eff} = 404.66 \times 10^{-26}$ cm^3 for the transition Eu^{3+}: $^5D_0 \rightarrow {}^7F_2$. CIE1931 coordinates obtained from the PL

spectra were also exposed in the reddish-orange region for all glasses. Moreover, the $\lambda_{exci.} = 394$ nm was the most dominant excitation giving rise to the intense red spectral emissions with higher lifetime values in the studied (E1–E1G3.0) Ba–Bi–B glasses. These properties make the investigated glasses a potential candidate for red-laser applications.

Declaration of competing interest

The authors declare that they have no known competing financial interests or personal relationships that could have appeared to influence the work reported in this paper.

Acknowledgement

This work was supported by research fund of Chungnam National University.

Appendix A. Supplementary data

Supplementary data to this article can be found online at https://doi.org/10.1016/j.ceramint.2022.10.208.

References

[1] M. Yamane, Y. Asahara, Glasses for Photonics, Cambridge University Press, Cambridge, 2000, https://doi.org/10.1017/CBO9780511541308.
[2] T. Justel, H. Nikol, C. Ronda, New developments in the field of luminescent materials for lighting and displays, Angew. Chem. Int. Ed. 34 (1998) 3084–3103, https://doi.org/10.1002/(SICI)1521-3773(19981204)37:22<3084::AID-ANIE3084>3.0.CO;2-W.
[3] N.C. George, K.A. Denault, R. Seshadri, Phosphors for solid state white lighting, Annu. Rev. Mater. Res. 43 (2013) 481–501, https://doi.org/10.1146/annurev-matsci-073012-125702.
[4] S. Tanabe, Rare-earth-doped glasses for fiber amplifiers in broadband telecommunication, Compt. Rendus Chem. 5 (2002) 815–824, https://doi.org/10.1016/S1631-0748(02)01449-2.
[5] N. Kumamoto, D. Nakauchi, T. Kato, Go Okada, N. Kawaguchi, T. Yanagida, Photoluminescence, scintillation and thermally-stimulated luminescence properties of Tb-doped 12CaO-7Al_2O_3 single crystals grown by FZ method, J. Rare Earths 35 (2017) 957–963, https://doi.org/10.1016/S1002-0721(17)60999-2.
[6] J. Zhao, L. Huang, T. Liang, S. Zhao, S. Xu, Luminescent properties of Eu^{3+} doped heavy tellurite scintillating glasses, J. Lumin. 205 (2019) 342–345, https://doi.org/10.1016/j.jlumin.2018.09.045.
[7] C. Cascales, R. Balda, J. Fernandez, M.A. Arriandiaga, J.M. Fdez-Navarro, Fluorescence line narrowing spectroscopy of Eu^{3+} in TeO_2–TiO_2–Nb_2O_5 glass, Opt. Mater. 31 (2009) 1092–1095, https://doi.org/10.1016/j.optmat.2017.12.018.
[8] S. Yue Zi, Chen, Z. Xing Wen, X. Sha Peng, G. Abbas Ashraf, R. Fei Wei, T. Pang, Hai Guo, Transparent heavily Eu^{3+}-doped boroaluminate glass for X-ray detection, Ceram. Int. 48 (1) (2022) 947–952, https://doi.org/10.1016/j.ceramint.2021.09.179.
[9] L.M. Marcondes, S. Helena Santagneli, D. Manzani, F. Castro Cassanjes, G. Batista, V. Gacha Mendoza, C. Ramos da Cunha, G. Yves Poirier, M. Nalin, High tantalum oxide content in Eu^{3+}-doped phosphate glass and glass-ceramics for photonic applications, J. Alloys Compd. 842 (2020), 155853, https://doi.org/10.1016/j.jallcom.2020.155853.
[10] M. De, S. Jana, Optical characterization of Eu^{3+} doped titanium barium lead phosphate glass, Optik 215 (2020), 164718, https://doi.org/10.1016/j.ijleo.2020.164718.
[11] R. Nakamori, N. Kawano, A. Takaku, D. Nakauchi, H. Kimura, M. Akatsuka, K. Shinozaki, T. Yanagida, Preparation and scintillation properties of the Eu^{3+}-activated SrO–Al_2O_3–TeO_2 glasses, Mater. Res. Bull. 145 (2022), 11547, https://doi.org/10.1016/j.materresbull.2021.111547.
[12] X. Yang, J. Chen, S. Zheng, C. Chen, A downshifting Eu^{3+} doped glass embedded with concave pyramid microstructure to improve the efficiency of silicon solar cell, J. Rare Earths 38 (2020) 1158–1164, https://doi.org/10.1016/j.jre.2019.11.013.
[13] V. Venkatramu, P. Babu, C.K. Jayasankar, Fluorescence properties of Eu^{3+} ions doped borate and fluoroborate glasses containing lithium, zinc and lead, Spectrochim. Acta, Part A 63 (2006) 276–281, https://doi.org/10.1016/j.saa.2005.05.010.
[14] K. Marimuthu, S. Surendra Babu, G. Muralidharan, S. Arumugam, C.K. Jayasankar, Structural and optical studies of Eu^{3+} ions in alkali borate glasses, Phys. Status Solidi 206 (2009) 131–139, https://doi.org/10.1002/pssa.200824198.
[15] K. Swapna, Sk Mahamuda, A. Srinivasa Rao, T. Sasikala, P. Packiyaraj, L. Rama Moorthy, G. Vijaya Prakash, Luminescence characterization of Eu^{3+} doped zinc alumino bismuth borate glasses for visible red emission applications, J. Lumin. 156 (2014) 80–86, https://doi.org/10.1016/j.saa.2014.01.025.
[16] B. Deva Prasad Raju, C. Madhukar Reddy, Structural and optical investigations of Eu^{3+} ions in lead containing alkali fluoroborate glasses, Opt. Mater. 34 (2012) 1251–1260, https://doi.org/10.1016/j.optmat.2012.01.027.
[17] S. Gopi, S.K. Jose, A. George, N.V. Unnikrishnan, C. Joseph, P.R. Biju, Luminescence and phonon sideband analysis of Eu^{3+} doped alkali fluoroborate glasses for red emission applications, J. Mater. Sci. Mater. Electron. 29 (2018) 674–682, https://doi.org/10.1007/s10854-017-7961-8.
[18] M. Rajesh, G. Rajasekhara Reddy, N. JohnSushma, G. Devarajulu, B. Deva Prasad Raju, Phonon sideband analysis, structural and spectroscopic properties of Eu^{3+} ions embedded SiO_2–B_2O_3–CaF_2–NaF–Na_2O glasses, Opt. Mater. 107 (2020), 110038, https://doi.org/10.1016/j.optmat.2020.110038.
[19] N. Vijaya, C.K. Jayasankar, Structural and spectroscopic properties of Eu^{3+}-doped zinc fluorophosphate glasses, J. Mol. Struct. 1036 (2013) 42–50, https://doi.org/10.1016/j.molstruc.2012.09.037.
[20] R. Priyanka, S. Arunkumar, Ch Basavapoornima, R.M. Mathelane, K. Marimuthu, Structural and spectroscopic investigations on Eu^{3+} ions doped boro-phosphate glasses for optical display applications, J. Lumin. 220 (2022), 116964, https://doi.org/10.1016/j.jlumin.2019.116964.
[21] J. Sankar Roy, Y. Messaddeq, Photoluminescence study of Eu^{3+} doped zinc-tungsten-antimonite glasses for red LED applications, J. Lumin. 228 (2020), 117608, https://doi.org/10.1016/j.jlumin.2020.117608.
[22] M. De, S. Jana, S. Mitra, Structural and spectroscopic characteristics of Eu^{3+} embedded titanium lead phosphate glasses for red luminescence, Solid State Sci. 114 (2021), 106560, https://doi.org/10.1016/j.solidstatesciences.2021.106560.
[23] C. Bin Deng, M. Zhang, T. Lan, Min-Jun Zhou, Y. Wen, J. Zhong, Xin-Yuan Sun, Spectroscopic investigation on Eu^{3+}-doped TeO_2-Lu_2O_3-WO_3 optical glasses, J. Non-Cryst. Solids 554 (2021), 120565, https://doi.org/10.1016/j.jnoncrysol.2020.120565.
[24] S.H. Nandyala, G. Hungerford, J.D. Santos, B.M. Walsh, L. Di Silvio, A. Stamboulis, Time-resolved and excitation-emission matrix luminescence behaviour of boro-silicate glasses doped with Eu^{3+} ions for red luminescent application, Mater. Res. Bull. 140 (2021), 111340, https://doi.org/10.1016/j.materresbull.2021.111340.
[25] K. Mariselvam, R. Arun Kumar, M. Jagadeesh, Spectroscopic properties and Judd-Ofelt analysis of Eu^{3+} doped barium bismuth fluoroborate glasses, Opt. Mater. 84 (2018) 427–435, https://doi.org/10.1016/j.optmat.2018.07.044.
[26] Y. Kondo, K. Tanaka, R. Ota, T. Fujii, Yo-ichi Ishikawa, Time-resolved study of luminescence in soda-lime silicate glasses co-doped with Gd^{3+} and Eu^{3+}, Opt. Mater. 27 (2005) 1438–1444, https://doi.org/10.1016/j.optmat.2004.10.007.
[27] N. Pawlik, B. Szpikowska-Sroka, A.S. Swinarew, M. Łezniak, W.A. Pisarski, Structural and optical properties of Eu^{3+}/Gd^{3+} ions in silica xerogels and powders obtained by solegel method, J. Mol. Struct. 1126 (2016) 29–36, https://doi.org/10.1016/j.molstruc.2016.03.095.
[28] N. Wantana, E. Kaewnuam, B. Damdee, S. Kaewjaeng, S. Kothan, H.J. Kim, J. Kaewkhao, Energy transfer based emission analysis of Eu^{3+} doped Gd_2O_3-CaO-SiO_2-B_2O_3 glasses for laser and X-rays detection material applications, J. Lumin. 194 (2018) 75–81, https://doi.org/10.1016/j.jlumin.2017.10.004.
[29] I. Khan, G. Rooh, R. Rajaramakrishna, N. Sirsittipokakun, H.J. Kim, C. Wongdeeying, J. Kaewkhao, Development of Eu^{3+} doped Li_2O-BaO-GdF_3-SiO_2 oxyfluoride glass for efficient energy transfer from Gd^{3+} to Eu^{3+} in red emission solid state device application, J. Lumin. 203 (2018) 515–524, https://doi.org/10.1016/j.jlumin.2018.07.009.
[30] B. Damdee, K. Kirdsiri, H.J. Kim, K. Yamanoi, A. Angnanon, N. Triamnak, S. Kothan, J. Kaewkhao, Effect of Gd_2O_3 concentration on X-rays induced and photoluminescence characteristics of Eu^{3+}- Activated Gd_2O_3–B_2O_3 glass, Radiat. Phys. Chem. 189 (2021), 109681, https://doi.org/10.1016/j.radphyschem.2021.109681.
[31] P. Ramakrishna, R.K. Padhi, D.K. Mohapatra, Hrudananda Jena, B.S. Panigrahi, Structural characterization, $Gd^{3+} \rightarrow Eu^{3+}$ energy transfer and radiative properties of Gd/Eu in codoped Li_2O–ZnO–SrO–B_2O_3–P_2O_5 glass, Opt. Mater. (2022), https://doi.org/10.1016/j.optmat.2022.112060, 1202060.
[32] M.A. Marzouk, F.H. ElBatal, H.A. ElBatal, Effect of TiO_2 on the optical, structural and crystallization behavior of barium borate glasses, Opt. Mater. 57 (2016) 14–22, https://doi.org/10.1016/j.optmat.2016.04.002.
[33] A.S. Abouhaswa, Hesham M.H. Zakaly, Shams A.M. Issa, M. Rashad, M. Pyshkina, H.O. Tekin, R. El-Mallawany, Mostafa Y.A. Mostafa, Synthesis, physical, optical, mechanical, and radiation attenuation properties of TiO_2–Na_2O–Bi_2O_3–B_2O_3 glasses, Ceram. Int. 47 (2021) 185–204, https://doi.org/10.1016/j.ceramint.2020.08.122.
[34] H. Ticha, L. Tichy, On the estimation of the refractive index of heavy metal oxide glasses, Mater. Chem. Phys. 278 (2022), 125638, https://doi.org/10.1016/j.matchemphys.2021.125638.
[35] T. Alharbi, H.F.M. Mohamed, Y.B. Saddeek, A.Y. El-Haseib, Kh S. Shaaban, Study of the TiO_2 effect on the heavy metals oxides borosilicate glasses structure using gamma-ray spectroscopy and positron annihilation technique, Radiat. Phys. Chem. 164 (2019), 08345, https://doi.org/10.1016/j.radphyschem.2019.108345.
[36] L. Zur, J. Janek, M. Sołtys, J. Pisarska, W.A. Pisarski, Effect of BaF_2 content on luminescence of rare-earth ions in borate and germanate glasses, J. Am. Ceram. Soc. 99 (2016), https://doi.org/10.1111/jace.14223, 2009–2016.
[37] J. Yuan, W. Wang, Y. Ye, T. Deng, D. Ou, J. Cheng, S. Yuan, P. Xiao, Effect of BaF_2 variation on spectroscopic properties of Tm^{3+} doped gallium tellurite glasses for efficient 2.0 μm laser, Front. Chem. 8 (2021), 628273, https://doi.org/10.3389/fchem.2020.628273.
[38] B.R. Judd, Optical absorption intensities of rare-earth ions, Phys. Rev. 37 (1962) 750–761, https://doi.org/10.1103/PhysRev.127.750.
[39] G.S. Ofelt, Intensities of crystal spectra of rare-earth ions, J. Phys. Chem. 37 (1962) 511–520, https://doi.org/10.1063/1.1701366.
[40] O.I. Sallam, A.M. Madbouly, N.A. Elalaily, F.M. Ezz-Eldin, Physical properties and radiation shielding parameters of bismuth borate glasses doped transition metals,

J. Alloys Compd. 843 (2020), 156056, https://doi.org/10.1016/j.jallcom.2020.156056.
[41] G.V. Prakash, R. Jagannathan, D.N. Rao, Physical and optical properties of NASICON-type phosphate glasses, Mater. Lett. 57 (2002) 134–140, https://doi.org/10.1016/S0167-577X(02)00719-X.
[42] A. Duffy, A common optical basicity scale for oxide and fluoride glasses, J. Non-Cryst. Solids 109 (1989) 35–39, https://doi.org/10.1016/0022-3093(89)90438-9.
[43] V. Dimitrov, S. Kim, T. Yoko, S. Sakka, Third harmonic generation in PbO-SiO_2 and PbO-B_2O_3 glasses, J. Ceram. Soc. Jpn. 101 (1993) 59–63, https://doi.org/10.2109/jcersj.101.59.
[44] N.M. Bobkova, Properties and structure of bismuth-borate glasses (review), Glass Ceram. 72 (2016) 360–365, https://doi.org/10.1007/s10717-016-9790-2.
[45] L. Singh, V. Thakur, R. Punia, R.S. Kundu, A. Singh, Structural and optical properties of barium titanate modified bismuth borate glasses, Solid State Sci. 37 (2014) 64–71, https://doi.org/10.1016/j.solidstatesciences.2014.08.010.
[46] A. Kumar Yadav, P. Singh, A review of the structures of oxide glasses by Raman spectroscopy, RSC Adv. 5 (5) (2015), 67583, https://doi.org/10.1039/c5ra13043c.
[47] M. Veeramohan Rao, V.V. Ravi Kanth Kumar, Nk Shihab, D. Narayana Rao, Z-Scan studies of barium bismuth borate glasses, Opt. Mater. 84 (2018) 178–183, https://doi.org/10.1016/j.optmat.2018.06.066.
[48] E.A. Davis, N.F. Mott, Conduction in non-crystalline systems V. Conductivity, optical absorption and photoconductivity in amorphous semiconductors, Phil. Mag. 22 (1970) 903–922, https://doi.org/10.1080/14786437008221061.
[49] K. Mariselvam, J. Liu, Synthesis and luminescence properties of Eu^{3+} doped potassium titano telluroborate (KTTB) glasses for red laser applications, J. Lumin. 230 (2021), 117735, https://doi.org/10.1016/j.jlumin.2020.117735.
[50] F. Urbach, The long-wavelength edge of photographic sensitivity and of the electronic absorption of solids, Phys. Rev. 92 (1953) 1324, https://doi.org/10.1103/PhysRev.92.1324.
[51] M. Wachtler, A. Speghini, S. Pigorini, R. Rolli, M. Bettinelli, Phonon sidebands and vibrational properties of Eu^{3+} doped lead germanate glasses, J. Non-Cryst. Solids 217 (1997) 111–114, https://doi.org/10.1016/S0022-3093(97)00282-2.
[52] C.K. Jørgensen, R. Reisfeld, Judd-Ofelt parameters and chemical bonding, J. Less Common Met. 93 (1983) 107–112, https://doi.org/10.1016/0022-5088(83)90454-X.
[53] M.H.V. Werts, R.T.F. Jukes, J.W. Verhoeven, The emission spectrum and the radiative lifetime of Eu^{3+} in luminescent lanthanide complexes, Phys. Chem. Chem. Phys. 4 (2002) 1542–1548, https://doi.org/10.1039/B107770H.
[54] N. Thi, Q. Lien, N. Ngoc Trac, P. Van Do, Ho Van Tuyen, Judd-Ofelt analysis of Eu^{3+} and adjustable emission in Eu^{3+}/Eu^{2+} co-doped sodium aluminosilicate glasses, J. Phys. Chem. Solid. 164 (2022), 110637, https://doi.org/10.1016/j.jpcs.2022.110637.
[55] P. Aryal, H.J. Kim, A. Khan, S. Saha, S.J. Kang, S. Kothan, Y. Yamsuk, J. Kaewkhao, Development of Eu^{3+}-doped phosphate glass for red luminescent solid-state optical devices, J. Lumin. 227 (2020), 117564, https://doi.org/10.1016/j.jlumin.2020.117564.
[56] K. Linganna, C.K. Jayasankar, Optical properties of Eu^{3+} ions in phosphate glasses, Spectrochim. Acta, Part A 97 (2012) 788–797, https://doi.org/10.1016/j.saa.2012.07.031.
[57] Sk Mahamuda, P. Sailaja, K. Swapna, M. Venkateswarlu, A.S. Rao, Enhanced red emission in Eu^{3+} ions doped ZnO-Al_2O_3-BaF_2-CaF_2-B_2O_3 glasses for visible laser applications, J. Non-Cryst. Solids 577 (2022), 121306, https://doi.org/10.1016/j.jnoncrysol.2021.121306.
[58] P. Ramesh, V. Hegde, K. Keshavamurthy, A.G. Pramod, G. Jagannath, D. Abdullah Aloraini, A.H. Almuqrin, M.I. Sayyed, K.S. Harisha, S. Khan, K. Annapurna, S. Venugopal Rao, M.K. Kokila, Influence of gamma irradiation on photoluminescence and nonlinear optical properties of Eu^{3+} activated heavy metal borate glasses, Opt. Mater. 116 (2021), 111102, https://doi.org/10.1016/j.optmat.2021.111102.
[59] P. Meejitpaisan, C. Kedkaew, J. Kaewkhao, Spectroscopic properties of Eu^{3+}-doped gadolinium calcium phosphate and fluorophosphates glasses, Mater. Today 5 (2018) 13926–13933, https://doi.org/10.1016/j.matpr.2018.02.042.
[60] A.N. Meza-Rocha, I. Camarillo, R. Lozada-Morales, U. Caldino, Reddish-orange and neutral/warm white light emitting phosphors: Eu^{3+}, Dy^{3+} and Dy^{3+}/Eu^{3+} in potassium-zinc phosphate glasses, J. Lumin. 183 (2017) 341–347, https://doi.org/10.1016/j.jlumin.2016.11.068.
[61] CIE, CUPC, Commission internationale de l'eclairage proceedings, Cambridge University, Cambridge, 1931 (1932).
[62] C.S. McCamy, Correlated color temperature as an explicit function of chromaticity coordinates, Color Res. Appl. 17 (1992) 142–144, https://doi.org/10.1002/col.5080170211.